Isoniazid-Gentisic acid cocrystallization: Solubility, Stability, Dissolution rate, Antioxidant and Flowability Properties Studies

Syed Muddassir Ali Mashhadi[1,2*], Andrei S. Batsanov[2], Syed Arslan Sajjad[3], Yasir Nazir[1,4], Moazzam Hussain Bhatti[1] and Uzma Yunus[1]*

[1] Department of Chemistry, Allama Iqbal Open University, Islamabad, Pakistan.
[2] Department of Chemistry, Durham University, Stockton Road, Durham DH1 3LE, United Kingdom.
[3] Department of Pharmacy, Bahauddin Zakariya University, Multan, Pakistan.
[4] Institute for Molecular Bioscience, University of Queensland, Australia.

* Corresponding author.
uzma_yunus@yahoo.com
muddassir_bakie@yahoo.com

Abstract

Isoniazid (INH) is a key antitubercular agent, which exhibits poor chemical stability in the solid state associated with the hydrazide group. Cocrystallization with Gentisic Acid having antioxidant activity, may produce solid forms with improved pharmaceutical properties. The complementary nature of the functional groups of isoniazid and the chosen coformer resulted in success for cocrystal formation. Cocrystal (INH-Gentisic acid) was characterized by solid-state NMR, DSC, PXRD and single crystal-XRD. The synthesized cocrystals were tested for the inhibition of synthetic-free radicals, DPPH. INH-Gentisic acid demonstrated high free radical scavenging activity against DPPH (78.36% for 125µg/ml concentration) which were better than that of ascorbic acid (37.16%) used as standard. Moreover solubility, stability and flowability properties of the synthesized cocrystals are optimized.

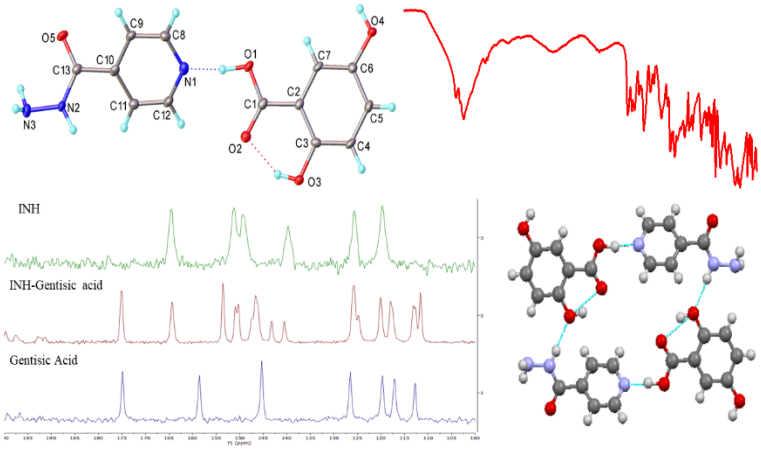

Keywords: Cocrystal, Isoniazid, Gentisic Acid, Physico-chemical properties, Antioxidant studies, Flowability studies

Introduction

Tuberculosis (TB) is considered as a global emergency by World Health Organization (WHO). Fixed-dose combinations (FDCs) based on first line anti-TB drugs are recommended by

International Union against Tuberculosis and Lung Diseases (IUATLD) for the use to avert monotherapy as well as drug resistance.[1],[2] Oxidative stress during TB leads to hepatotoxicity during the treatment with first-line anti-TB drugs like INH, pyrazinamide and Rifampicin (RIF). Oxidation reactions causes the degradation of APIs or tablets in solid form effecting the stability and shelf life of pharmaceutical formulations. Antioxidants herbal medicines have shown decreased oxidative stress significantly leading to the prediction of positive role of antioxidant drugs during anti-TB treatment. [3],[4],[5]

Isoniazid[6] (INH) is a very efficient remedy against *M. tuberculosis* recommended by WHO. It is first line primary constituent in different FDCs and 'triple therapy'' being used to counter tuberculosis since 1952. FDCs including RIF and INH have shown apprehension that RIF demonstrate alarmingly decreased bioavailability and tablet degradation which can lead to therapy failure.[7] RIF and INH yield isonicotinyl hydrazone (HYD) after interacting in solid formulation during storage of solid anti-TB FDC formulations under enhanced stability test conditions.[8] Moisture absorbance by tablet containing INH and ethambutol was also marked under accelerated stability test conditions.[9] These facts leads to subsided efficiency of FDCs and needs the attention.

Pharmaceutical cocrystals renders an opportunity to synthesize a single crystalline form consisting of multiple pharmaceutically important compounds.[10] Cocrystals are multi-component solids held together by non-covalent forces like hydrogen bonding which is well studied interaction leading to desired altered[11] physicochemical and stability properties of APIs.[12],[13] Screening of cocrystals can be achieved either by solution-based or solid-state methods. Solution based procedure involve the slow evaporation of suitable solvent leading to crystallization while the other is based on grinding without (neat grinding approach) or with the addition of a small amount of solvent (solvent-assisted grinding approach).[14]

The supramolecular synthon[15] knowledge is important to engineer the synthesis of cocrystals. INH is remarkably prone to forming cocrystals with other organic molecules: a survey of the Cambridge Structural Database[16] (version 5.41, November 2019) revealed 55 such structures. INH potential as a supramolecular building block[17] is primarily due to its pyridine N atom and the hydrazide group being complementary with carboxylic acid and hydroxyl groups, which allows to design particularly stable synthons.[18] Bernstein and co-workers[19-21] systematically studied cocrystals of INH with carboxylic acids, prospective for pharmaceutical applications, and showed the most stable heterosynthon to be an INH-acid pair linked by strong C(O)OH···N(pyridine) hydrogen bond (synthon *D*). Hydroxyl derivatives of benzoic acid, which have antioxidant properties, are thus complementary, and ideal for

cocrystallization, with INH.[22] INH cocrystals with Vanillic acid and Caffeic acid, have shown increased stability when tested under increased humidity and temperature conditions replacing INH in FDCs.[23, 24]. Cocrystals of INH with antioxidants may provide relief in oxidative stress in patients of Tuberculosis during treatment and increases tabletting shelf life[23,25,26] as well. Gentisic (dihydroxybenzoic) acid is an active metabolite of salicylic acid degradation and a by-product of tyrosine and benzoate metabolism. It is biologically active and show anti-inflammatory, antirheumatic and antioxidant properties. Gentisic acid is readily oxidised and is used as an antioxidant excipient in pharmaceutical preparations.[27] It also readily forms cocrystals, with 37 structures available in CSD. In the present study a cocrystal of INH with Gentisic acid (Scheme 1) was prepared, utilizing both the latter's supramolecular complementarity with INH and its antioxidant activity.

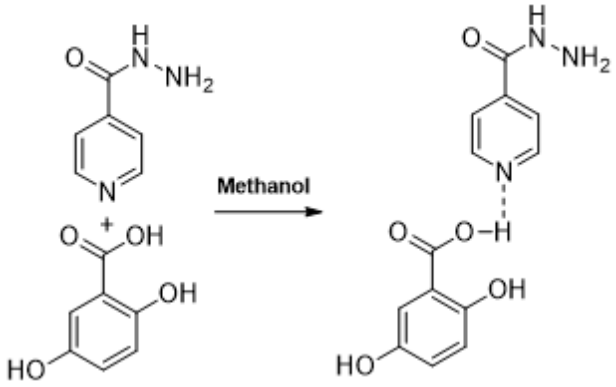

Scheme 1: Synthetic scheme for cocrystallization of INH-Gentisic acid

Solid-state NMR has recently been applied for the structural insight of cocrystals[28] and can be used as complementary technique to X-ray diffraction.[29,30] The field of NMR crystallography leverages the synergy between experimental and CASTEP calculated chemical shifts. The field of charge–density studies, developed and boosted by advances in hardware, provides opportunity to map electron density in a crystal and provide accurate results in the calculation of NMR chemical shielding constants for the compounds in the solid state.[31]

Experimental

Isoniazid and Gentisic acid were purchased from Sigma-Aldrich and used without further purification.

Synthesis

INH-Gentisic acid cocrystal was obtained by dissolving 1:1 molar ratio of coformer and INH separately in methanol. Both solutions were mixed and heated at 55 ^{o}C for 15 minutes with

stirring and left at room temperature. Slow evaporation lead to the formation of off white small crystals after seven days which were filtered and dried without washing.

Infrared spectroscopy

The IR spectra were recorded on Varian 640-IR spectrophotometer.

Differential Scanning Calorimeter

Differential Scanning Calorimetry (DSC) experiments were performed by heating from 30 to 300°C at 10°C per minute in a standard aluminum pan in an inert atmosphere (helium) on Perkin Elmer DSC 8500 instrument. DSC experiments were carried out to study the thermal behavior of the cocrystals. Melting point can be determined from the melting curve. If the low temperature side of melting peak is almost a straight line, the melting point corresponds to the onset and if melting curve are concave in shape the melting point are characterized by the peak maxima.

Solid-State NMR Spectroscopy

Bruker Avance III HD spectrometer was used to obtain the ^{13}C solid state NMR spectra by using ^{13}C resonant frequency of 125.7 MHz at 11.7 Tesla magnetic field strength. Nearly 100 mg of solid sample was packed into a 4 mm rotor made of zirconia equipped with a Kel-F cap. The pulse sequence for cross polarization at magic angle spinning (CP-MAS) was used for acquisition of spectra. Spinning rate for rotor was set at 10.00 kHz. Magic angle was set by calibration using KBr. Spectra were obtained using 180 seconds recycle delay and 320 number of scans were taken for cocrystal while the same parameters for INH were 600 seconds and 120 scans respectively. Data sets were Fourier transformed with line broadening factor at 5 Hz and phase corrected to yield frequency-domain spectra. Indirect reference to neat tetramethylsilane (TMS) was made for the chemical shifts by setting the high frequency adamantane signal at 38.5 ppm.

^{1}H NMR spectra were also obtained under fast MAS conditions and were acquired using rotors of the size of 1.3 at 40.0 kHz MAS frequency and ^{1}H NMR frequency of 500 MHz. The chemical shifts were referenced indirectly to neat TMS by setting the adamantane signal at 1.9 ppm. There was no noticeable difference in ^{1}H resolution consistent with the relatively weak dependence of resolution on MAS rate and the likely significant contribution of susceptibility effects to ^{1}H line widths in these samples.

X-ray crystallography

Powder X-ray diffraction pattern (2θ range 3-55° at step size 0.02°) was measured at room temperature on a Bruker D8 Advance diffractometer equipped with a Lynx-eye Soller PSD detector and variable slits, using Cu-$K\alpha_{1,2}$ radiation (λ = 1.5418 Å). Polycrystalline samples produced by grinding single crystals were sprinkled onto Si slides covered with a thin layer of Vaseline.

Single-crystal diffraction experiment was carried out on a Bruker 3-circle D8 Venture diffractometer with a PHOTON 100 CMOS area detector, using Mo-K_α radiation (λ=0.71073 Å) from Incoatec IμS micro source with focusing mirrors. The crystal was cooled to 120 K using a Cryostream (Oxford Cryosystems) open-flow N_2 gas cryostat. The data were processed using APEX3 v.2016.1-0 software. Reflection intensities were integrated using SAINT v8.38A software (Bruker AXS, 2017) and corrected for absorption by semi-empirical method based on Laue equivalents and multiple scans, using SADABS 2016/2 program.[32] The structures were solved by dual-space intrinsic phasing method using SHELXT 2018/2 program,[33] and refined by full-matrix least squares using SHELXL 2018/3 software[34] on OLEX2 platform.[35] All non-H atoms were refined in anisotropic approximation, all H atoms were revealed from difference Fourier map and refined in isotropic approximation. Crystallographic data in CIF format (including structure factors) have been deposited with the Cambridge Crystallographic Data Centre, CCDC-1980680. Energies of intermolecular interactions in the crystal were calculated in B3LYP/6-31G(d,p) mode, using CrystalExplorer software.[36,37]

Crystal data: $C_7H_6O_4 \cdot C_6H_7N_3O$ (M = 291.26 g/mol), triclinic, space group $P\bar{1}$ (no. 2), a = 3.7075(6), b = 10.9505(18), c = 15.966(3) Å, α = 101.366(6), β = 95.706(6), γ = 91.327(6)°, V = 631.72(18) Å^3, Z = 2, T = 120 K, μ(Mo-$K\alpha$) = 0.12 mm^{-1}, D_{calc} = 1.531 g/cm^3, 8870 reflections with 2Θ ≤ 50° measured, 2229 unique (R_{int} = 0.050), 243 refined parameters, R_1 = 0.038 on 1655 reflections with $I > 2\sigma(I)$, wR_2 = 0.093 on all data.

CASTEP calculations

GIPAW method implemented in CASTEP version 17.2 was used for first principles.[38] PBE functional[39] was used for calculations and on-the-fly-generated ultra-soft pseudopotentials, with cut off 600 eV energy. Atomic positions were optimized with the center of mass and unit cell parameters fixed as their single crystal XRD-determined values, with integrals taken over the Brillouin zone using a Monkhorst–Pack grid with a maximum k-point sample spacing of 0.1 A^{-1}. Co-ordinate input files were generated from starting CIF files using CIF2cell.[40] Crystallographically distinct atoms in the output magres files[41] are labelled using the labels in the input CIF files. The NMR parameters were calculated[42,43] using the same k-point

sampling and cut-off energy. The resulting ^{13}C shielding values were transformed into chemical shifts by using 164.4 ppm as reference value.

Solubility, Stability and Dissolution rate studies

Solubility, Stability and Dissolution rate studies were carried out spectrophotometrically and UV-1700, Shimadzu, Japan, equipped with 1.0 cm quartz cuvettes. 200−600 nm range was used for this purpose.

Solubility determination

Solubility studies of INH-Gentisic acid cocrystal was performed in duplicate according to method reported by Higuchi and Connors.[44] In this saturation solubility study, an excess quantity of INH and its cocrystal was placed in the vials containing 5 mL of buffer at pH 7.4. The vials were agitated on shaker (125 agitations / min) for 24 hrs at room temperature (25 ^{o}C). The solution was then filtered through syringe filter and the amount of the drug dissolved was analysed spectrophotometrically. Concentrations of solutions was determined by UV/vis spectrometry and separate linear calibration curve was plotted for cocrystal and INH in the range from 339 nm to 266 nm.

Stability determination

Stability studies of INH and INH-Gentisic acid cocrystal were performed in duplicate by placing known amount of INH and Cocrystals in oven at 80 ^{o}C for 24 hrs and then amount of the drug and cocrystals was determined spectrophotometrically.

Dissolution rate determination

Dissolution rate were determined by dissolving known amount of INH and INH-Gentisic acid separately in buffer solution of pH 7.4, Alloquate of 1mL were taken after fixed time intervals using syringe filter, equal amount of buffer solution was also added to keep the amount of solution constant. Concentration of the solutions were determined spectrophotometrically.

Flowability properties studies

Carr's Index and Hausner Ratio

Compressibility (Carr's) index and Hausner ratio calculation is easy, fast, and popular mean to predict flow characteristics of pharmaceuticals. It is indirect measurement for size/shape, bulk density, surface area, moisture and cohesiveness of the investigated materials.

The known masses of INH-Gentisic acid was taken in the measuring cylinder, apparent volume was noted for the calculation of bulk density. Later the measuring cylinder was tapped for 500 times and the tapped volume and tapped density was noted. Carr's index and Hausner ratio were determined from the measured values using the equations.

$$Compressibility\ Index = 100 \times \left[\frac{\rho_{tapped} - \rho_{bulk}}{\rho_{tapped}}\right]$$

$$Hausner\ Ratio = 100 \times \left[\frac{\rho_{tapped}}{\rho_{bulk}}\right]$$

Angle of repose

Resistance to particle movement is calculated by angle of repose and give the qualitative picture of the internal cohesive and frictional factors. Triturated sample are made to free fall along the walls of a funnel under the action of gravity. The funnel is fixed at a specified height and the compounds are made to fall in such a way that they form a heap. The procedure is continued until the apex of heap touches the tip of funnel, the radius of the heap is calculated and from radius and height, angle of repose is measured by using the following equation.

$$Angle\ of\ repose(\theta) = tan^{-1}\left(\frac{h}{r}\right)$$

Free radical scavenging/antioxidant assay studies

The DPPH (2,2- diphenyl-1-picrylhydrazyl) free radical scavenging assay was used to find out free radical scavenging abilities of the synthesized cocrystal.[45] 0.1mM DPPH control solution was prepared in ethanol which was then diluted to adjust its absorbance to 0.70 (at 515 nm). Sample solutions were prepared by dissolving 1mg/ml from each compounds in ethanol followed by double dilution. 2ml of DPPH is added to each compound-containing 1mg/ml solutions and incubated in dark for 20min at 37^{o}C. To calculate the percent scavenging of DPPH radical by INH-Gentisic acid following equation was used. Absorbance was recorded by using VARIAN, CARY 50 Bio. UV-Visible spectrophotometer at 515nm. Antioxidant activity was determined with the help of following formula.

%age Inhibition = B-S/B × 100

"B" represents the absorbance of the reference/control (DPPH) and "S" represents the sample absorbance.

Results and Discussion

INH-Gentisic acid cocrystal was synthesized and the solid form was confirmed to be cocrystals by characterization using spectroscopic, thermal and X-ray diffraction techniques.

IR studies

IR spectrum (Figure 1) of INH showed the stretching of –NH bond in the high wave number region of the IR at 3360 cm^{-1}, while the cocrystal showed a sharp band of weak intensity at 3340 cm^{-1}. Another sharp band was present at 3088cm^{-1}, which was attributed to the C-H (aromatic) stretching vibrations while INH showed at 3172 cm^{-1} for the same bond. C=O

stretching vibration was present at 1667 cm^{-1} for cocrystal while at 1670 cm^{-1} for INH. C=N stretching was observed at 1600 cm^{-1} for cocrystal and that of INH. Aromatic ring vibrations were attributed at 1510 cm^{-1}, 1445 $cm^{-1}$for cocrystal and at 1500 cm^{-1},1465 cm^{-1} for INH. Pyridine ring of cocrystal was identified at 1409 cm^{-1} while the same was identified at 1410 for INH.

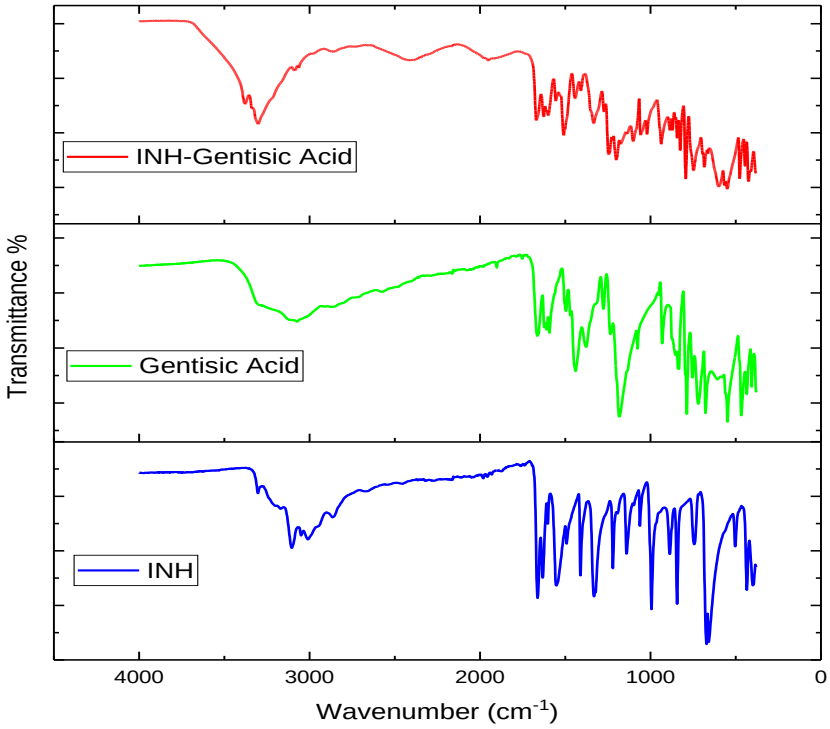

Figure 1: IR spectra of coformers and Cocrystal

DSC studies

DSC results of Cocrystal of isoniazid and Gentisic acid expressed endothermic peak at 178^{o}C. Single transition showed the sharp melting point as expressed in Figure 2.

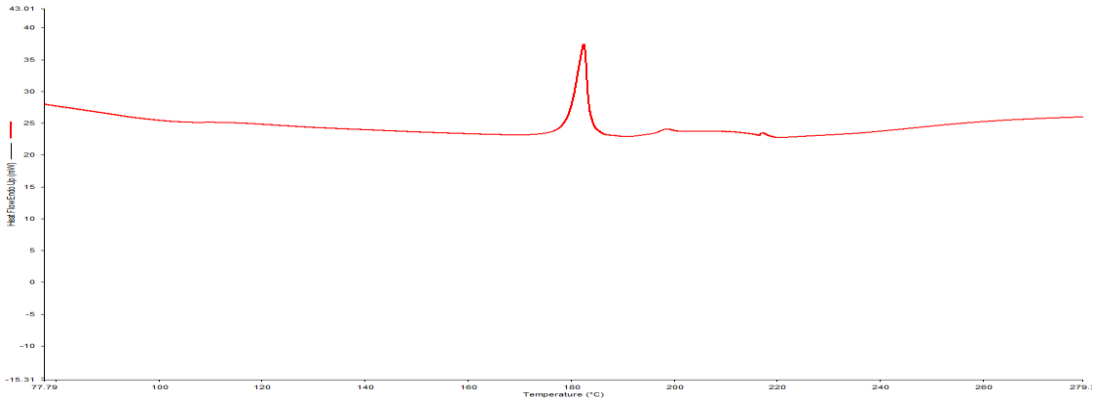

Figure 2: DSC result for INH-Gentisic acid Cocrystal

PXRD Studies

Sharp peaks (Figure 3) depicts the high crystallinity in the structure. Calculated and experimental results were in agreement reasonably. A weak peak at low 2-theta and some peaks at high 2-theta do not match the simulated patterns. This showed some impurities from coformers in the bulk sample.

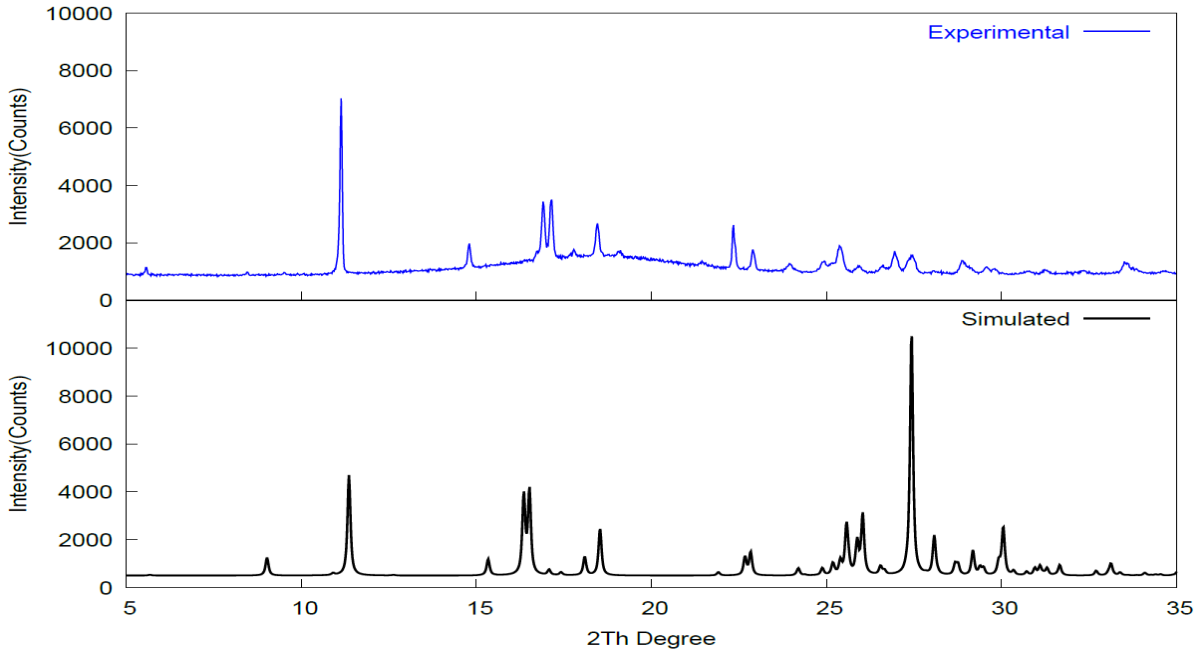

Figure 3: Experimental and Simulated PXRD results for INH-Gentisic acid Cocrystal

Single crystal XRD studies

INH and Gentisic acid co-crystallize, in equimolar ratio, in a triclinic structure (space group $P\bar{1}$). The asymmetric unit contains one pair of neutral molecules (Figure 4), hydrogen-bonded into a *D*-type synthon.[46] A network of strong hydrogen bonds (Table 1) links these into a quilled layer parallel to the (1 1 0) plane (Figure 5). The remarkable feature of the structure, setting it apart from all previously reported INH-acid cocrystals,[19-21] is the chessboard arrangement of the component molecules, so that all strong hydrogen bonds (except the intramolecular OH···O in the acid) and all synthons are *hetero*-molecular. The estimated energies of intermolecular interactions (Table 1) show that synthon *D* is indeed the strongest-bound, as Bernstein el al. have inferred,[19] mainly by electrostatic and polarization terms. The next strongest interactions are between coplanar molecules of INH and the acid in the [1 $\bar{1}$ 0] direction, while the interaction at the 'step' of the layer are much weaker and in the same region, one of the supposedly 'active' H atoms at N(3) surprisingly does not participate in any hydrogen bond. Formally, the most energetically favorable synthon is the $R_4^4(28)$ tetramer

(highlighted in Figure 5a) with the total intermolecular energy of ca. 180 kJ mol^{-1}, followed by tetramers $R_6^6(26)$, $R_4^4(14)$ and $R_4^4(20)$ (170, 106 and 96 kJ mol^{-1}, respectively).

The layers are held together mainly by van der Waals (dispersive) interactions: both the INH and the Gentisic acid molecules form segregated π-π stacks with like molecules of adjacent layers (related by the translation *a*). The stacks are slanted, with uniformly separated parallel aromatic rings. The interplanar separations are 3.44 Å in INH stacks and 3.32 Å in the acid stacks, with the intermolecular energies of -19.8 kJ mol^{-1} in either case. The INH conformation is similar to that in pure solid,[21] apart from stronger twist about the C(10)–C(13) bond, 34.1(2)° *vs* 17.8°.

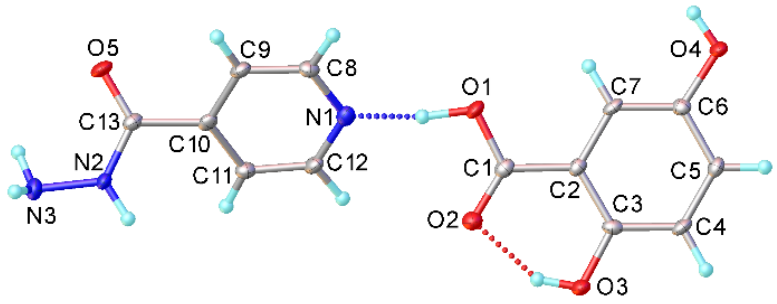

Figure 4: Asymmetric unit in the INH-Gentisic acid cocrystal (= synthon *D*). Atomic displacement ellipsoids are drawn at the 50% probability level. The pyridine and carboxylic planes are inclined by 31.6(1)° and the C(12)H···O(2) distance (2.86(2) Å) exceeds the sum of van der Waals radii

Table 1. Hydrogen Bonds D-H···A and total intermolecular energies in INH-Gentisic acid Cocrystal

D	H	A	d(D-H)/Å	d(H-A)/Å	d(D-A)/Å	D-H-A/°	E_{tot} /kJ mol^{-1}
O(1)	H(1)	N(1)	1.07(2)	1.54(2)	2.603(2)	172(2)	-50.7
O(3)	H(3)	O(2)	0.89(2)	1.76(2)	2.558(2)	148(2)	--
O(4)	H(4)	O(5)[1]	0.88(3)	1.86(3)	2.740(2)	173(2)	-39.2
N(2)	H(2)	O(3)[2]	0.90(2)	2.01(2)	2.906(2)	176(2)	-34.4
N(3)	H(3B)	O(4)[3]	0.91(2)	2.21(2)	3.114(2)	168(2)	-15.8

Symmetry transformations: [1] 1–*x*, 1–*y*, 1–*z*; [2] 2–*x*, –*y*, 1–*z*; [3] *x*, *y*, 1+*z*

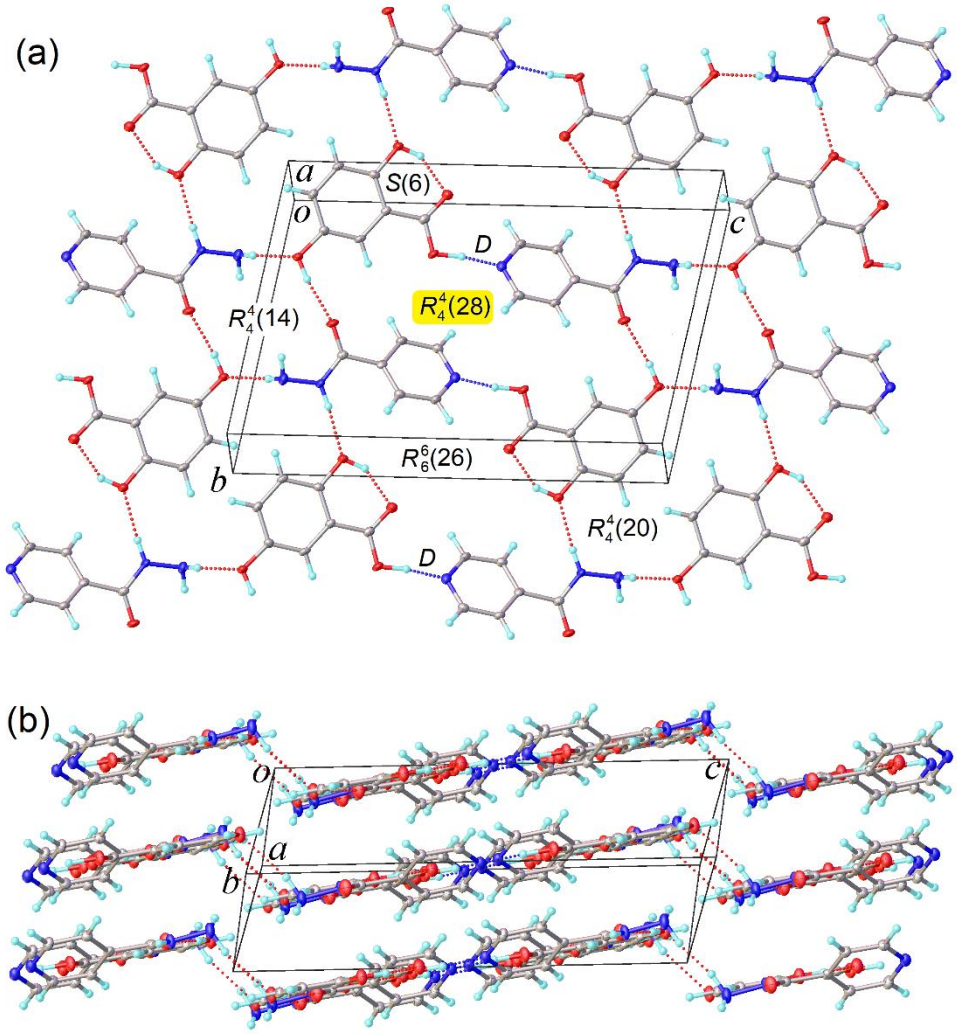

Figure 5: Crystal packing in INH-Gentisic acid cocrystal, showing hydrogen bonds (dotted lines) and synthon notation: (a) a layer projected onto (1 1 0) plane, (b) side-view of the layers.

Solid state NMR and CASTEP-calculated spectral Studies

Phase-pure material containing peaks corresponding to the INH-Gentisic acid cocrystal structure was detected. No additional peaks corresponding to unreacted coformers were identified. Comparison of experimental and CASTEP calculated ^{13}C NMR spectrum (Figure 6) and ^{1}H NMR spectrum revealed good agreement (Figure 7).

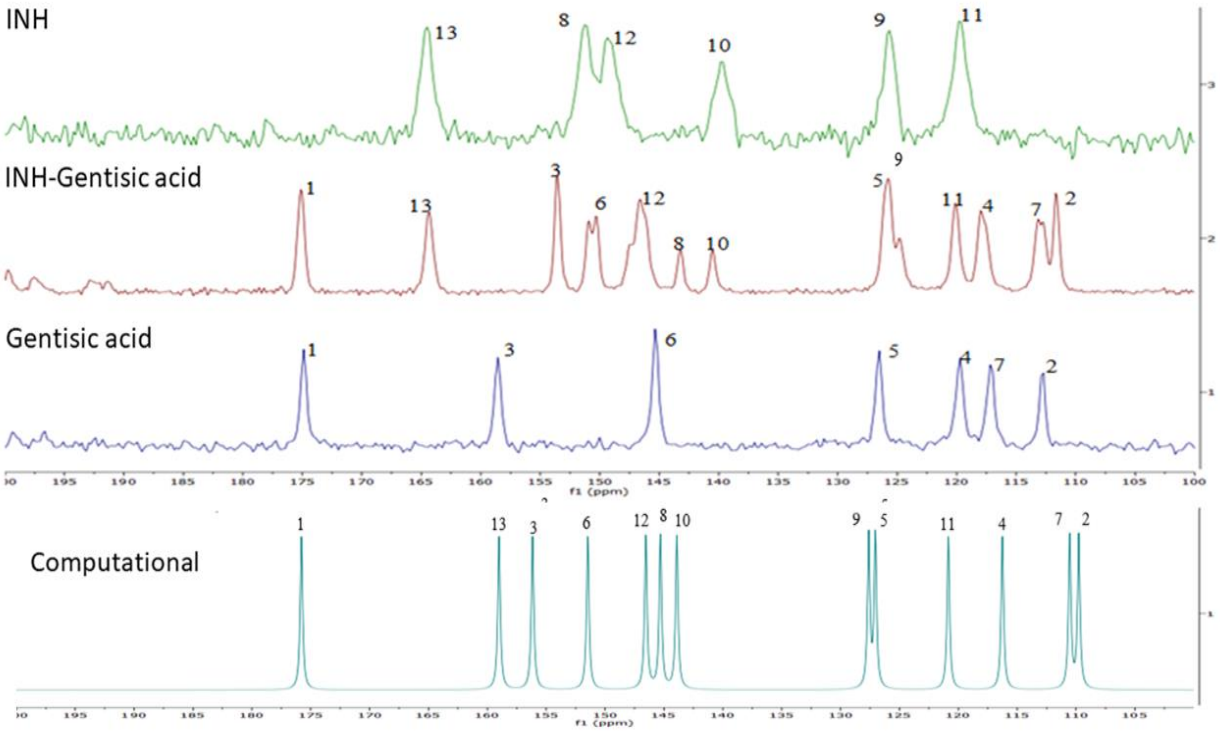

Figure 6: ^{13}C solid state NMR spectrum of INH-Gentisic acid cocrystal, comparison of experimental and CASTEP calculated ^{13}C NMR spectrum

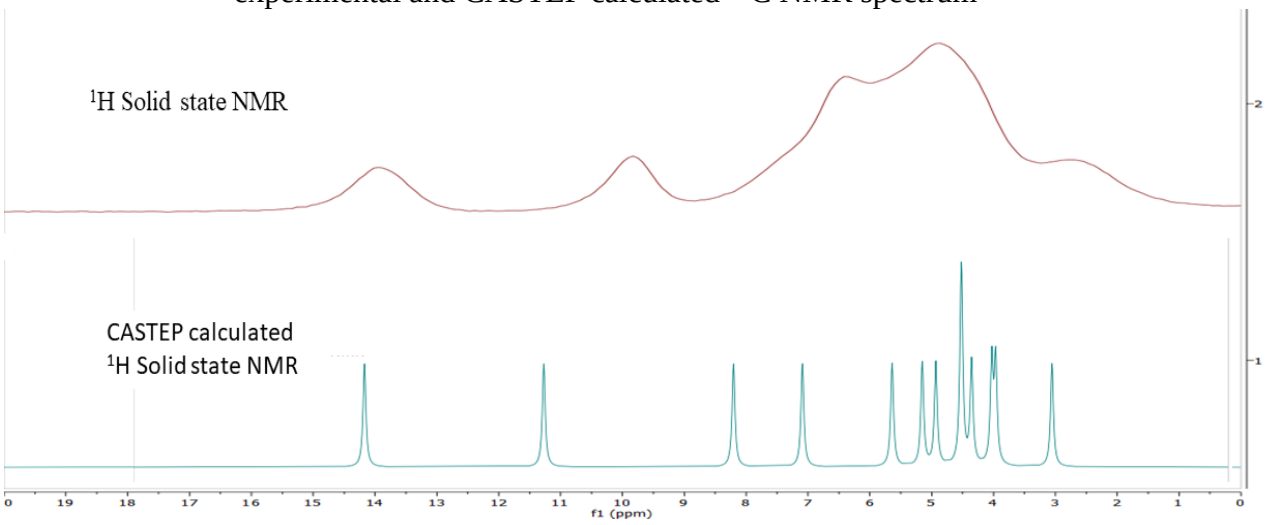

Figure 7: Comparison of Experimental and CASTEP calculated solid state ^{1}H NMR

Reference shielding of 164.4 ppm was used which gave better overall agreement in the CSTEP calculated and experimental results. Comparison of results is arranged in Table 2.

Table 2: Comparison of CASTEP calculated and Experimental chemical shifts

Label	INH-Gentisic acid Cocrystal	
	Expt	Calc

C1	175.1	175.8
C10	140.5	143.9
C11	120.1	120.8
C12	147.1	146.5
C13	164.4	159.0
C2	111.6	109.8
C3	153.5	156.2
C4	117.8	116.3
C5	124.7	127.0
C6	150.5	151.5
C7	112.9	110.5
C8	143.2	145.3
C9	**125.8**	**127.6**

Calculated ^{15}N shieldings were also able to identify all N atoms present in the INH-Gentisic acid cocrystal shieldings are arranged in Table 3.

Table 3: CASTEP calculated shielding***** for N-NMR

Label	INH-Gentisic cocrystal
N1	-60.1
N2	70.8
N3	159.9

*****These are shieldings rather than referenced shifts.

Solubility, Stability and Dissolution rate studies

The INH-Gentisic acid cocrystal showed 7.71 mg/mL solubility in pH 7.4 buffer solution was very less as compared to that of Isoniazid with solubility 76.30 mg/mL under the same conditions applied. The INH-Gentisic acid cocrystal was fairly stable up to 74.99% at 80 ^{o}C when placed for 24 hours. INH-Gentisic acid cocrystal exhibited comparable stability to that of INH whose stability is 83.86% (Table 4). Most of the component was dissolved in solution in about 4 minutes as shown by the data in Table 5 and the graph (Figure 8).

Table 4: solubility and stability results for INH-Gentisic acid Cocrystal

Sample	Physical Appearance	Melting Point (°C)	Stability at 80°C for 24 hrs	Solubility (in buffer pH 7.4)	λ_{max}
INH	White crystal	172°C	83.86%	76.30 mg/mL	263 nm
Gentisic Acid	White powder	199.5 °C	-	-	-
INH-Gentisic acid cocrystal	Brown Prism	178°C	74.99%	7.71 mg/mL	324.6 nm

Table 5: Dissolution rate studies for INH-Gentisic acid cocrystal

Sample No.	Time (minutes)	Measured Absorbance	Concentration (mg/mL)
1	1	0.456	0.807
2	3	0.521	0.922
3	5	0.549	0.972
4	10	0.563	0.996
5	50	0.605	1.070

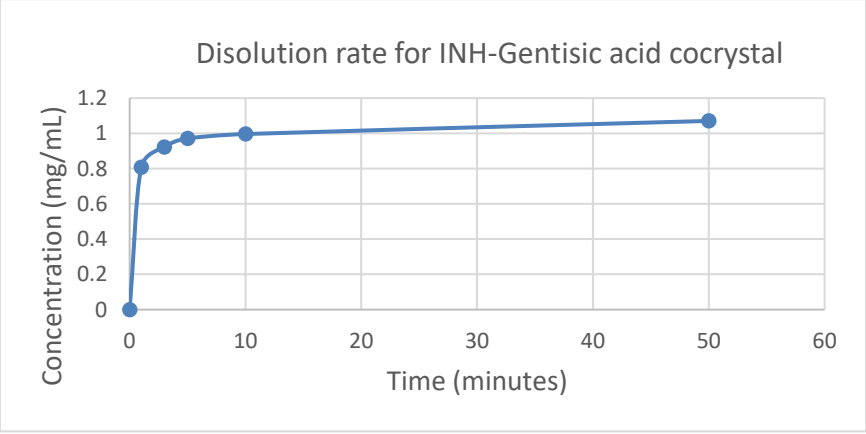

Figure 8: Dissolution rate of INH-Gentisic acid Cocrystal

Flowability properties studies

Cocrystal showed less density when compared to that of INH, however the studied properties are in pharmaceutically acceptable ranges and are shown in Table 6.

Table 6: Flowability properties for INH-Gentisic acid Cocrystal

Code	Bulk density (mg/ml)	Tapped density(mg/ml)	Hausner ratio	Carr's index	Angle of repose
INH	819.67	961.54	1.2	15%	21°
INH-Gentisic acid Cocrystal	129.6	203.7	1.6	36%	40°

Free radical scavenging/antioxidant assay studies

The antioxidant potential of the synthesized bioactive cocrystals were studied using DPPH assay. This assay is based on the ability of an antioxidant to scavenge DPPH free radicals. C9 showed highest scavenging activity with 78.36 % inhibition at 125µg/ml concentration compared to reference ascorbic acid with %age inhibition 37.16% at this concentration. The results are are summarized in table 7.

Table 7: Antioxidant Activity results for INH-Gentisic acid Cocrystal

Compound	Concentration (µg/ml)	% age Inhibition
INH-Gentisic acid cocrystal	1000	66.12
	500	73.35
	250	**79.56**
	125	**78.36**
Ascorbic Acid	1000	90.46
	500	89.19
	250	63.89
	125	37.16

Conclusion

Isoniazid (INH) forms cocrystal with hydroxyl derivatives of benzoic acids (Gentisic acid) due to complementary nature of the functional groups of INH and Gentisic acid. Cocrystal form was characterized by solid-state NMR, DSC, PXRD and single crystal-XRD. Cocrystal demonstrated free radical scavenging activity against DPPH (78.36% for 125µg/ml concentration) which was better than that of ascorbic acid (37.16%). Antioxidant and flowability properties suggest that cocrystal may have improved storage stability as hydrazide functional group is masked by hydrogen bonding which causes degradation of Rifampicin and antioxidant properties hence cocrystal may replace INH in FDCs used to treat tuberculosis.

Acknowledgements

We are thankful to HEC Pakistan for providing funding for this project and Durham University UK for Lab access.

We are also thankful Dr. Paul Hodgkinson and Dr. DC Apperley for their valuable suggestions during ^{13}C and ^{1}H NMR experiments and to W.D. Carswell for DSC experiments.

References

[1] H. Bhutani, S. Singh, K.C. Jindal, Drug-drug interaction studies on first-line anti-tuberculosis drugs, Pharm. Dev. Technol. 10 (2005) 517–524. https://doi.org/10.1080/10837450500299982.

[2] S.A. Carvalho, E.F. da Silva, M.V.N. de Souza, M.C.S. Lourenço, F.R. Vicente, Synthesis and antimycobacterial evaluation of new trans-cinnamic acid hydrazide derivatives, Bioorganic Med. Chem. Lett. 18 (2008) 538–541. https://doi.org/10.1016/j.bmcl.2007.11.091.

[3] S.M.A. Mashhadi, U. Yunus, M.H. Bhatti, I. Ahmed, M.N. Tahir, Synthesis, characterization, solubility and stability studies of hydrate cocrystal of antitubercular Isoniazid with antioxidant and anti-bacterial Protocatechuic acid, J. Mol. Struct. 1117 (2016) 17–21. https://doi.org/10.1016/j.molstruc.2016.03.057.

[4] I. Verma, S.K. Jindal, N.K. Ganguly, Studies on Respiratory Disorders, (2014) 101–114. https://doi.org/10.1007/978-1-4939-0497-6.

[5] N. Rehman, M. Khalid, M.H. Bhatti, U. Yunus, A.A.C. Braga, F. Ahmed, S.M.A. Mashhadi, M.N. Tahir, Schiff base of isoniazid and ketoprofen: Synthesis, X-ray crystallographic, spectroscopic, antioxidant, and computational studies, Turkish J. Chem. 42 (2018) 639–651. https://doi.org/10.3906/kim-1706-45.

[6] P. Mishra, J. Albiol-chiva, D. Bose, A. Durgbanshi, Optimization and Validation of a Chromatographic Method for the Quantification of Isoniazid in Urine of Tuberculosis Patients According to the European, (n.d.) 1–12. https://doi.org/10.3390/antibiotics7040107.

[7] C.J. Shishoo, S.A. Shah, I.S. Rathod, S.S. Savale, M.J. Vora, Impaired bioavailability of rifampicin in presence of isoniazid from fixed dose combination (FDC) formulation, Int. J. Pharm. 228 (2001) 53–67. https://doi.org/10.1016/S0378-5173(01)00831-6.

[8] H. Bhutani, S. Singh, K.C. Jindal, A.K. Chakraborti, Mechanistic explanation to the catalysis by pyrazinamide and ethambutol of reaction between rifampicin and isoniazid in anti-TB FDCs, J. Pharm. Biomed. Anal. 39 (2005) 892–899. https://doi.org/10.1016/j.jpba.2005.05.015.

[9] H. Bhutani, T.T. Mariappan, S. Singh, An Explanation for the Physical Instability of a Marketed Fixed Dose Combination (FDC) Formulation Containing Isoniazid and Ethambutol and Proposed Solutions, 30 (2004) 667–672. https://doi.org/10.1081/DDC-120039184.

[10] J.W. Steed, The role of co-crystals in pharmaceutical design, Trends Pharmacol. Sci. 34 (2013) 185–193. https://doi.org/10.1016/j.tips.2012.12.003.

[11] C.A. Gunawardana, C.B. Aakeröy, Co-crystal synthesis: Fact, fancy, and great expectations, Chem. Commun. 54 (2018) 14047–14060. https://doi.org/10.1039/c8cc08135b.

[12] N.K. Duggirala, M.L. Perry, Ö. Almarsson, M.J. Zaworotko, Pharmaceutical cocrystals: Along the path to improved medicines, Chem. Commun. 52 (2016) 640–655. https://doi.org/10.1039/c5cc08216a.

[13] M. Karimi-Jafari, L. Padrela, G.M. Walker, D.M. Croker, Creating Cocrystals: A review of Pharmaceutical Cocrystal Preparation Routes and Applications, Cryst. Growth Des. 18 (2018) 6370–6387. https://doi.org/10.1021/acs.cgd.8b00933.

[14] P. Saganowska, M. Wesolowski, DSC as a screening tool for rapid co-crystal detection in binary mixtures of benzodiazepines with co-formers, J. Therm. Anal. Calorim. 133 (2018) 785–795.

https://doi.org/10.1007/s10973-017-6858-3.

[15] G.R. Desiraju, Supramolecular Synthons in Crystal Engineering—A New Organic Synthesis, Angew. Chem. Int. Ed. Engl. 34 (1995) 2311–2327. https://doi.org/10.1002/anie.199523111.

[16] C.R. Groom, I.J. Bruno, M.P. Lightfoot, S.C. Ward, The Cambridge Structural Database. Acta Crystallogr. Sect. B Struct. Sci. 72 (2016) 171–179. https://doi.org/10.1107/S2052520616003954.

[17] D.J. Berry, J.W. Steed, Pharmaceutical cocrystals, salts and multicomponent systems; intermolecular interactions and property based design, Adv. Drug Deliv. Rev. 117 (2017) 3–24. https://doi.org/10.1016/j.addr.2017.03.003.

[18] S.M.A. Mashhadi, U. Yunus, M.H. Bhatti, M.N. Tahir, Isoniazid cocrystals with anti-oxidant hydroxy benzoic acids, J. Mol. Struct. 1076 (2014) 446–452. https://doi.org/10.1016/j.molstruc.2014.07.070.

[19] A. Lemmerer, J. Bernstein, V. Kahlenberg, One-pot covalent and supramolecular synthesis of pharmaceutical co-crystals using the API izoniazid: a potential supramolecular reagent. CrystEngComm, 12 (2010) 2856–2864. https://doi.org/10.1039/c000473a.

[20] A. Lemmerer, J. Bernstein, V. Kahlenberg, Hydrogen bonding patterns of the co-crystal containing the pharmaceutically active ingredient isoniazid and terephthalic acid. J. Chem. Crystallogr. 41 (2011) 991–997. https://doi.org/10.1007/s10870-011-0031-9.

[21] A. Lemmerer, Covalent assistance to supramolecular synthesis: modifying the drug functionality of the antituberculosis API isoniazid in situ during co-crystallization with GRAS and API compounds. CrystEngComm, 14 (2012) 2465–2478. https://doi.org/10.1039/c1ce06310c.

[22] I. Sarcevica, L. Orola, M. V. Veidis, A. Podjava, S. Belyakov, Crystal and molecular structure and stability of isoniazid cocrystals with selected carboxylic acids, Cryst. Growth Des. 13 (2013) 1082–1090. https://doi.org/10.1021/cg301356h.

[23] B. Swapna, M.K.C. Mannava, A. Nangia, J. Pharm. Sci. 107 (2018) 1667–1679. https://doi.org/10.1016/j.xphs.2018.02.014.

[24] S. Allu, K. Suresh, G. Bolla, M.K.C. Mannava, A. Nangia, Role of hydrogen bonding in cocrystals and coamorphous solids: indapamide as a case study, CrystEngComm 21 (2019) 2043–2048. https://doi.org/10.1039/C8CE01075G.

[25] N. Rastogi, K.S. Goh, L. Horgen, W.W. Barrow, Synergistic activities of antituberculous drugs with cerulenin and trans-cinnamic acid against Mycobacterium tuberculosis, FEMS Immunol. Med. Microbiol. 21 (1998) 149–157. https://doi.org/10.1016/S0928-8244(98)00044-3.

[26] S.M.A. Mashhadi, D. Yufit, H. Liu, P. Hodgkinson, U. Yunus, Synthesis and structural characterization of cocrystals of isoniazid and cinnamic acid derivatives, J. Mol. Struct. 1219 (2020) 128621. https://doi.org/https://doi.org/10.1016/j.molstruc.2020.128621.

[27] R.R. Tian, Q.H. Pan, J.C. Zhan, J.M. Li, S.B. Wan, Q.H. Zhang, W.D. Huang, Comparison of phenolic acids and flavan-3-ols during wine fermentation of grapes with different harvest times, Molecules. 14 (2009) 827–838. https://doi.org/10.3390/molecules14020827.

[28] H.E. Kerr, L.K. Softley, K. Suresh, P. Hodgkinson, I.R. Evans, Structure and physicochemical characterization of a naproxen-picolinamide cocrystal, in: Acta Crystallogr. Sect. C Struct. Chem. 73 (2017) 168–175. https://doi.org/10.1107/S2053229616011980.

[29] M.R. Chierotti, R. Gobetto, Solid-State NMR Studies on Supramolecular Chemistry, in: Supramolecular Chemistry: from Molecules to Nanomaterials, John Wiley & Sons, Ltd, 2012.

https://doi.org/10.1002/9780470661345.smc026.

[30] N.J. Vigilante, M.A. Mehta, A 13C solid-state NMR investigation of four cocrystals of caffeine and theophylline, Acta Crystallogr. Sect. C Struct. Chem. 73 (2017) 234–243. https://doi.org/10.1107/S2053229617000869.

[31] Ł. Szeleszczuk, D.M.I. Pisklak, M. Zielińska-Pisklak, I. Wawer, Effects of structural differences on the NMR chemical shifts in cinnamic acid derivatives: Comparison of GIAO and GIPAW calculations, Chem. Phys. Lett. 653 (2016) 35–41. https://doi.org/10.1016/j.cplett.2016.04.075.

[32] L. Krause, R. Herbst-Irmer, G.M. Sheldrick, D. Stalke, Comparison of silver and molybdenum microfocus X-ray sources for single crystal structure determination. J. Appl. Crystallogr. 48 (2015) 3–10. https://doi.org/10.1107/S1600576714022985.

[33] G.M. Sheldrick, SHELXT - Integrated space-group and crystal-structure determination. Acta Crystallogr. Sect. A Found. Crystallogr. 71 (2015) 3–8. https://doi.org/10.1107/S2053273314026370.

[34] G.M. Sheldrick, Crystal structure refinement with SHELXL. Acta Crystallogr. Sect. C Struct. Chem. 71 (2015) 3–8. https://doi.org/10.1107/S2053229614024218.

[35] O.V. Dolomanov, L.J. Bourhis, R.J. Gildea, J.A.K. Howard, H. Puschmann, OLEX2: A complete structure solution, refinement and analysis program. J. Appl. Crystallogr. 42 (2009) 339–341. https://doi.org/10.1107/S0021889808042726.

[36] C.F. Mackenzie, P.R. Spackman, D. Jayatilaka, M.A. Spackman, *CrystalExplorer* model energies and energy frameworks. IUCrJ, 4 (2017) 575–587. https://doi.org/10.1107/S205225251700848X.

[37] M.J. Turner, J.J. McKinnon, S.K. Wolff, D.J. Grimwood, P.R. Spackman, D. Jayatilaka, M.A. Spackman, *CrystalExplorer 17.5* (2017). University of Western Australia. http://hirshfeldsurface.net

[38] S.J. Clark, M.D. Segall, C.J. Pickard, P.J. Hasnip, M.I.J. Probert, K. Refson, M.C. Payne, First principles methods using CASTEP, Zeitschrift für Krist. 220 (2005) 567–570. https://doi.org/10.1524/zkri.220.5.567.65075.

[39] J.P. Perdew, K. Burke, M. Ernzerhof, Generalized gradient approximation made simple, Phys. Rev. Lett. 77 (1996) 3865–3868. https://doi.org/10.1103/PhysRevLett.77.3865.

[40] T. Björkman, CIF2Cell: Generating geometries for electronic structure programs, Comput. Phys. Commun. 182 (2011) 1183–1186. https://doi.org/10.1016/j.cpc.2011.01.013.

[41] S. Sturniolo, T.F.G. Green, R.M. Hanson, M. Zilka, K. Refson, P. Hodgkinson, S.P. Brown, J.R. Yates, Visualization and processing of computed solid-state NMR parameters: MagresView and MagresPython, Solid State Nucl. Magn. Reson. 78 (2016) 64–70. https://doi.org/10.1016/j.ssnmr.2016.05.004.

[42] C.J. Pickard, F. Mauri, All-electron magnetic response with pseudopotentials: NMR chemical shifts, Phys. Rev. B. 63 (2001) 2451011–2451013. https://doi.org/10.1103/physrevb.63.245101.

[43] J.R. Yates, C.J. Pickard, F. Mauri, Calculation of NMR chemical shifts for extended systems using ultrasoft pseudopotentials, Phys. Rev. B - Condens. Matter Mater. Phys. 76 (2007) 024401. https://doi.org/10.1103/PhysRevB.76.024401.

[44] T. Higuchi, K.A. Connors, Phase Solubility Techniques, in: C.N. Reilly (Ed.), Adv. Anal. Chem. Instrum., Interscience, 1965: pp. 117–212.

[45] M. Ovais, M. Ayaz, A.T. Khalil, S.A. Shah, M.S. Jan, A. Raza, M. Shahid, Z.K. Shinwari, HPLC-DAD finger printing, antioxidant, cholinesterase, and α-glucosidase inhibitory potentials of a novel plant Olax nana, BMC Complement. Altern. Med. 18 (2018) 1. https://doi.org/10.1186/s12906-017-2057-9.

[46] M.C. Etter, Encoding and Decoding Hydrogen-Bond Patterns of Organic Compounds, Acc. Chem. Res. 23 (1990) 120–126. https://doi.org/10.1021/ar00172a005.